ANALYTIC CALCULATIONS AND NUMERICAL SIMULATIONS OF BOX-CAR THERMAL WAVE IMAGES OF PLANAR SUBSURFACE SCATTERERS.

D.J.Crowther, L.D.Favro, P.K.Kuo and R.L.Thomas

Department of Physics and Institute for Manufacturing Research
Wayne State University
Detroit, Michigan 48202

INTRODUCTION

The purpose of this study is to improve the quality of thermal wave infrared (IR) images in terms of the real shape of the defect. Due to heat diffusion into the sample, thermal wave images are usually blurred, especially for deep defects or long times. Because of this feature the use of traditional image post-processing (gradient image, threshold...) to assess the size and the shape of the defect quite often leads to false results. In order to increase the accuracy in the shape recovery, we need to "unblur" the thermal wave image, i.e. to reverse or invert the blurring process. To do so, our approach is to model the physical process such that a space description of the defect is involved parametrically and from that model to invert the image.

MODELING

The defect is modeled as a planar scatterer which fits an important class of defects such as delaminations. It has been shown [1] that it is possible from a pulsed experiment to determine the depth of the defect. Therefore, we will assume that the scatterer is at a known depth, that the medium is semi-infinite, and that the sample is flash-heated on its front surface. The general heat transfer equation for this system can be solved by the use of the Green's function in the first order Born approximation. The result at the surface of the sample for a scatterer at a depth ℓ is given by:

$$\Delta T(x,y,t) = -\frac{A}{2\pi}\left(\frac{1}{4\pi\alpha t}\right)^{1/2}\frac{\partial}{\partial \ell}\iint dx'\,dy'\,\frac{e^{-\frac{\left[\left[(x-x')^2+(y-y')^2+\ell^2\right]^{1/2}+\ell\right]^2}{4\alpha t}}}{\left[(x-x')^2+(y-y')^2+\ell^2\right]^{1/2}}\,f(x',y') \qquad (1)$$

where $\Delta T(x,y,t)$ represents the contrast image of a defect at an instant t and α the diffusivity of the medium. The contrast image is the result of the subtraction of the

Review of Progress in Quantitative Nondestructive Evaluation, Vol. 11
Edited by D.O. Thompson and D.E. Chimenti, Plenum Press, New York, 1992

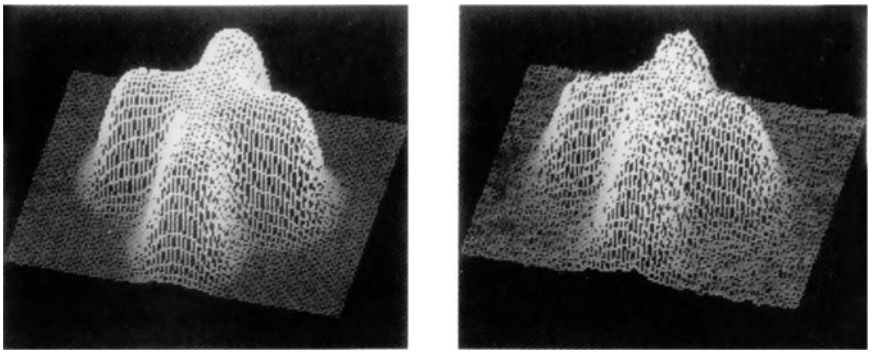

(a) (b)

Fig. 1. (a) 3-D perspective plot of a simulated thermal wave contrast image, and (b) an experimental thermal wave contrast image of a cross-shaped scatterer 0.75 mm deep in a stainless steel plate, 1 s after application of the heating pulse.

background from the thermal wave image. The function f(x',y') is the space description of the scatterer. The most important feature of this model is that the contrast image is calculated as a convolution of the "shape function" and a "heat spread function" which describes the way the heat has spread out in the sample from a point source at the instant t. The result of the convolution of those two images is a simulated thermal wave contrast image of the scatterer at the instant t. Figure 1(a) shows a comparison of the simulated contrast image of a cross-shaped flat bottom hole in a stainless steel plate and Fig. 1(b) shows the experimental contrast image of the actual sample under the same conditions . The cross is 25 mm end to end and represents a subsurface scatterer which is 0.75 mm deep. The images were simulated and measured for an access time of 1 s (following the heating pulse). The images have been normalized for comparison and are displayed as 3-D perspective plots.

INVERSION OF THERMAL WAVE IMAGES

As seen in Eq. (1), the shape function, f(x,y), is one of the functions which appears in the convolution. Therefore, the deconvolution of the contrast image (inverse Born approximation) should recover the shape of the scatterer.

Principle of the Deconvolution process

Before we attempt to deconvolve experimental images, we first use simulated contrast images (such as Fig.1(a)) to verify that the deconvolution is possible and to find the algorithm to be used for the shape recovery. The deconvolution can be separated into three distinct parts. First, we need to take the Fourier transform (i.e. go to the frequency domain) of the thermal wave contrast image and of the heat spread function, then secondly, proceed to the complex division of those two transforms. The result of this division is the Fourier transform of the shape of the scatterer. Finally, the shape itself is then given by doing the inverse Fourier transform of the result of the division (i.e. come back to the space domain). This procedure, when used with simulated contrast images faithfully recovers the original shape, confirming that our approach was correct in principle. Therefore, knowing

the heat spread function, it is possible to invert thermal wave images to determine the real shape of the scatterer from the blurred images. However, a practical difficulty comes from the finite level of digitization of the experimental images which are digitized at an 8-bit level in our experiment. In Fig. 2, we show the influence of 8-bit digitization of the simulated contrast image on the deconvolution result. Figure 1(a) shows the deconvolution result of a simulated contrast image (without any digitization prior to the deconvolution), and Fig. 2(b) shows the same simulated image, but on which an 8-bit digitization has been imposed before deconvolution. From Fig. 2(b), the shape of the scatterer would seem to have been lost, because of the imposed 8-bit truncation of the data. The source of this apparent loss may be found by examining Fig. 3, which shows the Fourier spectra of the images shown in Fig. 2. We notice that, in the frequency domain, the digitization of the image to be deconvolved introduces high frequency noise into the spectrum of the recovered shape. The lower the level of digitization, the more noise is introduced.

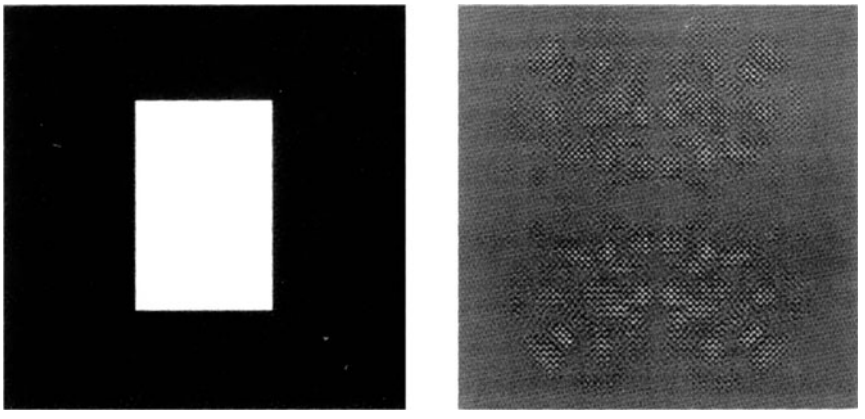

(a) (b)

Fig. 2. (a) Result of deconvolution of a simulated thermal wave contrast image of a rectangular scatterer, without artificial digitization, and (b) Deconvolution of the same image after an 8-bit truncation of the data.

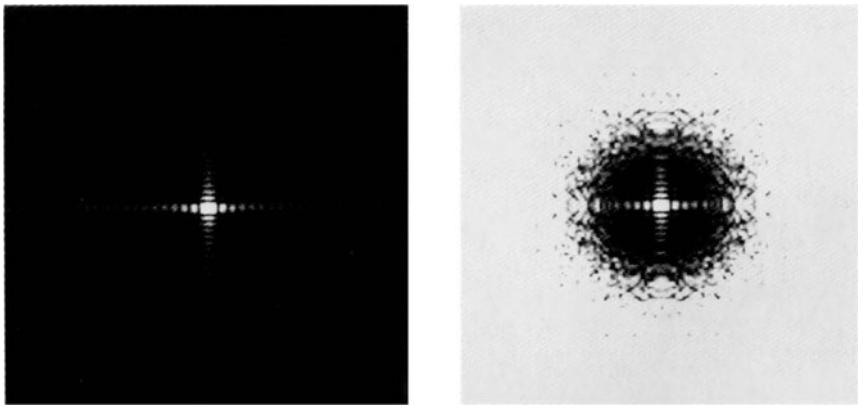

(a) (b)

Fig. 3. (a) Fourier transform of Fig. 2(a), and (b) Fourier transform of Fig. 2(b).

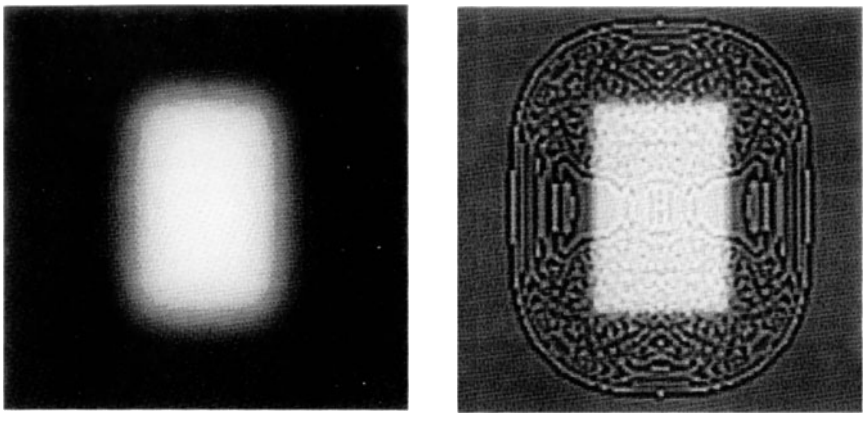

(a) (b)

Fig. 4. (a) Simulated contrast image of a rectangular scatterer and (b) Deconvolution result after an 8-bit truncation, and a Gaussian low-pass filter.

Although Fig. 2(b) seems to indicate that it is not possible to recover the shape of the scatterer after 8-bit digitization, we can see in Fig. 3(b) that the major features of the information relating to the shape are still there (center part of the Fig. 3(b)). The way to recover this hidden information is to apply a low pass filter to the 8-bit truncated image in the frequency domain. Figure 4(a) shows a truncated simulated contrast image and Fig. 4(b) the result of a Gaussian low- pass filter prior to the deconvolution of the image in Fig. 4(a). The filter is applied in the frequency domain at the beginning of the deconvolution process. The image is 128 pixels by 128 pixels, and the radius of the filter is 20 pixels. Because the high frequency components of the shape are masked by the digitization noise, we have lost the sharpness of the edges in Fig. 4(b), but most of the shape information has been successfully recovered.

Deconvolution of IR Experimental images

Next, we show shape recovery results for two experimental samples in which the scatterer is a flat bottom hole milled in the back side of the sample. In both samples the scatterer is 0.75 mm beneath the front surface. Results are presented for different times, i.e for different degrees of blurring. The first sample is a 20 mm thick Delrin plate in which the flat bottom hole is an 18 mm by 18 mm square with rounded corners. We show in Fig. 5(a) the experimental contrast images, and in Fig. 5(b), the corresponding recovered shapes for four access times (20, 30, 40 and 50 seconds). For the deconvolutions we used a Gaussian low-pass filter with radii of 17, 16, 14 and 10 pixels, respectively. We notice from Fig. 5 that, unlike the unprocessed thermal wave images, the recovered shapes are all square with rounded corners, a result which is faithful to the actual shape of the defect.

The second experimental sample to which we have applied this method is a 5 mm thick stainless steel plate with a 25 mm (end to end) cross-shaped flat bottom hole. It should be noted that the thermal wave images were taken with two different magnifications. Figure 6(a) shows two images at the first magnification for access times of 0.33 s and 0.83 s. To recover the shape of the cross, Fig. 6(b), we used Gaussian filters with radii of 9 and 7 pixels respectively. Notice that, although not observable in the unprocessed images, the left horizontal arm of the cross is wider than the right one in Fig. 6(b).

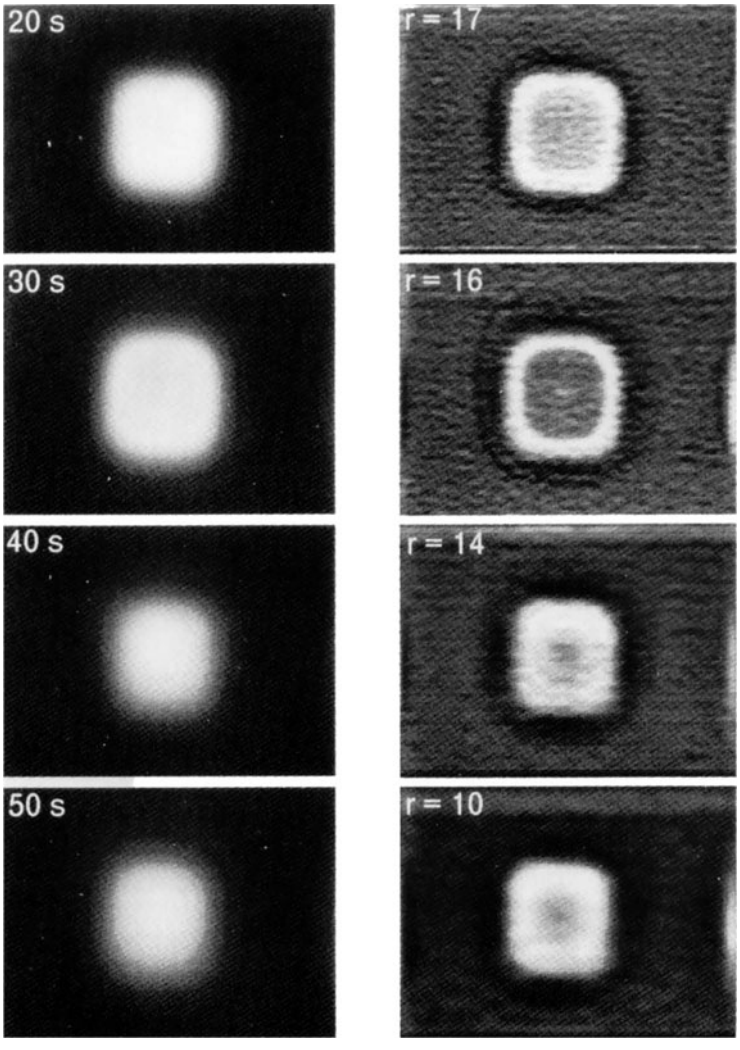

(a) (b)

Fig. 5. (a) Experimental (unprocessed) thermal wave contrast images of the square flat bottom hole at four access times of 20, 30, 40 and 50 seconds, and (b) Deconvolved shapes using Gaussian low-pass filters with radii of 17, 16, 14, and 10 pixels.

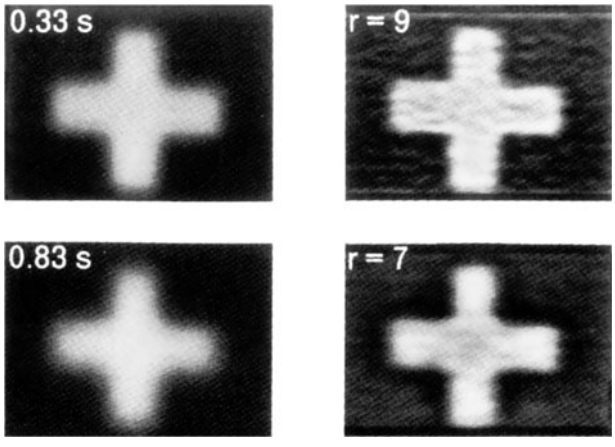

(a) (b)

Fig. 6. (a) Experimental (unprocessed) contrast images of the cross-shaped flat bottom hole at two different access times: 0.33 and 0.83 seconds, and (b) Deconvolved shapes for Gaussian low-pass filter radii of 9 and 7 pixels, respectively.

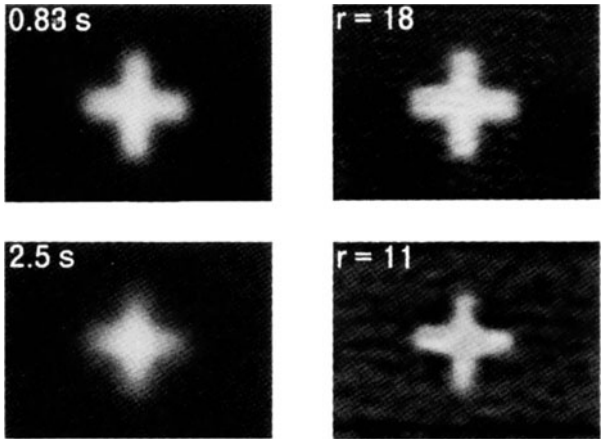

(a) (b)

Fig. 7. (a) Experimental (unprocessed) contrast images of the cross-shaped flat bottom hole at two different access times: 0.83 and 2.5 seconds, and (b) Deconvolved shapes for Gaussian low-pass filter radii of 18 and 11 pixels, respectively.

This is a very accurate recovery of the shape of the cross, which in fact does have a slightly wider left arm. This detail in shape recovery shows how accurate the inversion method can be. Two thermal wave images (access time 0.83 and 2.5 seconds) at a different magnification are presented Fig. 7(a) with their corresponding recovered shapes shown in Fig. 7(b). Even at these longer times, with greater blurring and poorer signal-to-noise ratios, we can see that the deconvolution method gives a reasonable assessment of the actual shape of the scatterer. Notice in particular that the thermal wave contrast image at 2.5 s is blurred to the point that it looks more like a diamond shape, and yet the recovered shape is still a recognizable cross.

CONCLUSION

We have described and demonstrated a new method to recover the shape of a subsurface scatterer using a thermal wave deconvolution process. Our method represents a promising means for significantly improving the spatial resolution of such thermal wave contrast images. Future work will be directed to improving the model by taking into account multiple scattering of the thermal waves to match the physical process more accurately, as well as refining the modeling of the defect by including thermal contact resistance. The resulting improvement in resolution should ultimately make thermal wave techniques competitive with other forms of imaging for NDE in terms of its capability for sizing and characterization of subsurface delaminations and other planar defects, such as disbonds in glue joints, welds, etc.

ACKNOWLEDGEMENTS

This work was sponsored by the Center for Advanced Nondestructive Evaluation, operated by Ames Laboratory, USDOE, for the Air Force Wright Aeronautical Laboratories under Contract No. W-7405-ENG-82 with Iowa State University, by the FAA Center for Aviation Systems Reliability and by the Institute for Manufacturing Research, Wayne State University.

REFERENCES

1. T. Ahmed, H.J. Jin, X. Wang, L.D. Favro, P.K. Kuo, and R.L. Thomas, in Review of Progress in Quantitative NDE, (Plenum Press, N.Y 1991), Vol. 10B.